Received: 7 November 2022 | Revised: 12 January 2023 | Accepted: 15 May 2023

DOI: 10.1002/jrs.6558

SPECIAL ISSUE - RESEARCH ARTICLE

Journal of RAMAN SPECTROSCOPY WILEY

Mineralogy of the LAR 12095 Martian shergottite as determined by micro-Raman and micro-X-ray fluorescence spectroscopies

Jennifer Huidobro | **Julene Aramendia** | **Cristina García-Florentino** | **Iratxe Población** | **Kepa Castro** | **Gorka Arana** | **Juan Manuel Madariaga**

Department of Analytical Chemistry, University of the Basque Country (UPV/EHU), Bilbao, Spain

Correspondence
Jennifer Huidobro, Department of Analytical Chemistry, University of the Basque Country (UPV/EHU), Barrio Sarriena s/n, 48940 Leioa, Spain.
Email: jennifer.huidobro@ehu.eus

Funding information
National Science Foundation (NSF); NASA; Raman On Mars project, Grant/Award Number: PID2019-107442RB-C31; Spanish Agency for Research; Strategic Project "Terrestrial and Planetary Alteration Processes", Grant/Award Number: UPV/EHU PES18/57; UPV/EHU

Abstract

In this work, the geochemical characterization of the olivine-phyric Martian shergottite LAR 12095 was performed by using two complementary analytical techniques: micro-Raman and micro-energy dispersive X-ray fluorescence spectroscopies. Thanks to this methodology, olivine, pyroxene, and ilmenite were detected as primary minerals from Mars. Maskelynite, hematite, anatase, chromite, merrillite, oxidized mackinawite, pyrrhotite, elemental sulfur, marcasite, jarosite, epsomite, and gypsum were classified as secondary minerals. The major novelty of this work is that alterations under anaerobic and aerobic conditions of S-bearing minerals can be appreciated. In this sense, primary sulfides were altered to secondary sulfides, elemental sulfur and sulfates under the oxygen-free Martian atmosphere. However, in the Earth's oxidizing atmosphere, primary sulfides are weathered to iron oxides, such as hematite. In addition, it should be highlighted that the presence of ilmenite, mackinawite, elemental sulfur, and jarosite has been reported for the first time in this meteorite.

KEYWORDS

LAR 12095 Martian meteorite, Mars, Martian sulfur cycle, mineralogy

1 | INTRODUCTION

Researchers study the formation and evolution of planets, such as Mars, by orbiters, rovers, landers, or studying rock samples. On the one hand, orbiters have recorded remotely the planet's mineralogy, geomorphology, and composition.[1] On the other hand, rovers and landers have performed fieldwork, using analytical techniques that have been able to analyze *in situ* the chemistry and mineralogy of Martian rocks and regolith. Tables 2 and 3 of the Huidobro et al.[2] review show the pros and cons of *in situ* analysis made by rovers, landers, and laboratory techniques. It has been found that *in situ* measurements have worse detection limits, limitations of the analysis due to environmental conditions, and lower precision and accuracy than laboratory techniques. Thus, in order to get better results, rock samples should also be analyzed in terrestrial laboratories. Until now, rocks from the

Martian surface can only be obtained from the ejected rocks that arrived to the Earth in the form of meteorites. Martian meteorites were traditionally divided into three main groups: shergottite, nakhlites, and chassignites (SNC). Moreover, SNC meteorites have been confirmed to belong to Mars on the basis of trapped noble gas compositions that match with Martian atmosphere.[3] The major group is that of shergottite, which represents the 83% of the total studied samples.[1]

However, the study of meteorites presents a handicap, and it is that they are often heavily weathered because these samples are mostly found in hot and cold deserts, where they have spent a considerable amount of time exposed to the terrestrial surface conditions. Therefore, identifying the origin of meteorite minerals has become a challenge because it is necessary to differentiate between primary, secondary, and terrestrial weathering minerals. This classification can be made based on the minerals already found on Mars by *in situ* analytical techniques and based on their chemical alterations. That is, primary minerals, as the name implies, are those that are originally from Mars and have not undergone any alteration. Secondary minerals are those that come from primary minerals because they have undergone alteration processes that caused a chemical change. Finally, as meteorites are found on the terrestrial surface, they may suffer further weathering processes. Thus detecting weathering minerals is crucial to identify which are the main processes that degrade meteorites on the Earth.

These minerals in meteorites, and their classification, can be determined using laboratory analytical techniques, giving also information about the history of the meteorite and consequently the history of Martian surface from where the meteorite was ejected. This knowledge will also help to analyze quickly the first Martian samples that will arrive to the Earth thanks to the Mars Sample Return (MSR) mission.[4]

Over time, traditional analytical techniques have been adapted to the era of *in situ* space exploration. In fact, research is always in progress in order to improve accuracy, miniaturization, precision, real-time measurements, automation, power consumption, reliability of operation under extreme conditions, and so forth.[2] Nowadays, more sophisticated analytical techniques have been used, especially those non-destructive ones with spectroscopic imaging capabilities, enhancing the characterization possibilities of meteorite samples at the micrometric level.

In this work, the shergottite LAR 12095 was selected to demonstrate the usefulness of using only two of those new non-destructive analytical techniques for its characterization: micro-Raman spectroscopy, in the point-by-point and imaging modes; and micro-energy dispersive X-ray fluorescence (μ-EDXRF) spectroscopy, mainly in the imaging mode.[5] The combination of μ-Raman spectroscopy and μ-EDXRF spectroscopy gives highly relevant results of the sample mineralogy, because they provide the elemental and the molecular characterizations respectively of the meteorite as well as the visualization of the distribution of minerals and elements on the surface of the meteorite.

Both techniques were selected in order to prove that the first *in situ* analytical technique on Mars (XRF spectroscopy), on board de Viking lander,[6] and the most novel technique to reach Mars (Raman spectroscopy), on board the Mars 2020 rover,[4] are a combination of techniques that give better results when used together.[7] In fact, both techniques are implemented in the last rover mentioned above. These techniques preserve the sample due to their non-destructive character giving complementary results especially when the elemental and molecular homogeneity need to be checked to guarantee representativeness of results.[8]

Therefore, the overall goal of this work is to characterize the mineralogy of the LAR 12095 Martian shergottite. Likewise, there are also different specific objectives: (1) to determine the primary, secondary, and weathering mineral phases; (2) to detect the possible processes occurring on Mars that caused the alteration of primary to secondary minerals in LAR 12095 Martian meteorite; (3) to identify the terrestrial processes that have weathered the meteorite; and (4) to prove that the combination of Raman and μ-EDXRF spectroscopy is one of the simplest and best performing combinations to study the mineralogy of meteorites.

2 | EXPERIMENTAL

2.1 | Sample

The Larkman Nunatak (LAR) 12095 Martian meteorite was found in 2012 in the Larkman Nunataks region of the Transantarctic Mountains, East Antarctica, by the US Antarctic Search for Meteorites program (ANSMET). The weight of the initial meteorite was 133.13 g and its dimensions were 5.5 × 3.8 × 3.4 cm. However, it was cut into thin sections for more detailed analysis. The measurements in this work were performed on a thin sample that weights 1.26 g and has dimensions of 1.3 × 1.0 × 0.2 cm, including the resin in which it is embedded. Both polished surfaces look similar to the naked eye, having a greenish gray matrix with some dark inclusions, separated by cracks and veins.

This sample was delivered to the IBeA Research Group of the University of the Basque Country (UPV/EHU) by a loan agreement between NASA's Johnson Space Center (JSC) and the UPV/EHU.

The initial characterization classified it as a Martian shergottite, according to the Meteoritical Bulletin.[9] Literature and the Meteoritical Bulletin reports that the LAR 12095 shergottite is composed by pyroxene (61–62 vol%), olivine (16–17 vol%), and maskelynite (21–23 vol%) groundmass. Minor phosphates (mainly merrillite, with rare apatite), oxides (1 vol%, chromite and Ti-magnetite), and sulfides (1 vol%, mainly Fe-rich pyrrhotite) are also present. In addition, microstructural features of shock metamorphism, including veins and darkened olivine are also observed.[9–12]

2.2 | Instrumentation

2.2.1 | Micro-Raman spectroscopy

The molecular characterization was performed using a Renishaw inVia confocal micro-Raman spectrometer (Renishaw, UK). The analyses were carried out both in single point mode and in the spectroscopic imaging mode. The instrument is equipped with a 785 (Renishaw, UK, RL785 with a nominal 45 mW out-put power) and 532 nm (Renishaw, UK, RL532C50 with a nominal 300 mW out-put power) excitation diode lasers and with a CCD detector cooled by Peltier effect. In addition, the instrument is coupled to a Leica DMLM microscope (Bradford, UK), implementing a XYZ Stage Control toolbar and equipped with a micro-camera for searching the points of interest. 5× N PLAN (0.12 NA), 20× N PLAN EPI (0.40 NA) lenses, and 50× N PLAN (0.75 NA) long-range objective were used for visualization and focusing. The nominal power of the source can be modulated between 0.1% and 100% of the total power to avoid thermo-decomposition of the sample. For this work, less than 20% was always used to preserve the sample. The spectra were obtained in the range of 150–1350 cm^{-1}, with an averaged spectral resolution of 1 cm^{-1}, accumulating several scans from each spectrum to improve the signal-to-noise ratio.

The Raman images were obtained using the high-resolution Stream Line™ setup (Renishaw, UK) coupled to the inVia Raman spectrometer. The control software moves the sample beneath the lens of the inVia's motorized microscope stage, so that the line is rastered across the region of interest with a spatial resolution down to 1 μm and moving in the *snake* mapping mode. The data are swept synchronously across the detector as the line moves across the sample and the spectra are read out continuously, recording a Raman spectrum at each pixel of the line raster.

The average spectral resolution is ±1 cm^{-1} in the spectral region of wavenumbers covered in these experiments. At the end, 2D Raman images are obtained containing individual Raman information at pixel level.

The inVia spectrometer was daily calibrated setting the 520.5 cm^{-1} silicon line. Data acquisition and treatment were carried out by the Wire™ 4.2 software package by Renishaw. The results were interpreted by comparing the collected Raman spectra with Raman spectra of pure standard compounds of the public databases RRUFF[13] and bibliography.

The measurement parameters (laser, laser power, number of accumulations, and the acquisition time of the spectra) were optimized for each analysis. Although both Raman lasers were used, better results were obtained with the 532 nm laser. This was because the sample is mainly silicate-bearing minerals and the use of the 785 nm laser promoted a luminescence phenomenon that mask other Raman signals, hiding valuable molecular information[14] as well as an offset in the baseline of the whole spectrum.

2.2.2 | μ-EDXRF spectrometer

The elemental characterization of the LAR 12095 Martian meteorite was performed using both single point analysis and hyper map capabilities of the μ-EDXRF spectrometer M4 Tornado (Bruker Nano GmbH, Berlin, Germany). This instrument has a micro-focus side window Rh tube powered by a low-power HV generator and cooled by air that extends to a maximum current of 700 μA and voltage of 50 kV. It implements a XFlash silicon drift detector with 30 mm^2 sensitive area and energy resolution of 145 eV for the Mn K-αline. The micrometric lateral resolution of the instrument, 25 μm for the K-α line, is achieved thanks to the polycapilar optics. The spot size varies as a function of the energy, being 17 μm at 2.3 KeV and 32 μm at 18.3 KeV. The focusing process is supported by two video microscopes, one of them explores the sample under a low magnification (1 cm^2 area) whereas the other performs the final focusing (1 mm^2 area). As the instrument can detect elements with an atomic number (Z) higher than 10 (starting from the sodium), the measurements were performed under vacuum (20 mbar) to enhance the detection of the lightest elements. A deconvolution of the signals in the sum spectrum representing the completely mapped area was conducted automatically to construct the elemental images. After that, the distribution map of each element was represented as a function of the intensity of each detected element K_α line, except for Pb, using in this case the L_β line. Elemental semi quantitative data of these images can also be obtained in the form of a table, but it should be highlighted that these results are semi-quantitative due to the method used is unspecific and is

based on the fitting of the elements detected in the spectrum. If quantitative data should be required, the method would be validated with certificate reference material. All the spectra acquisition and the image construction were performed using the M4 TORNADO software.

3 | RESULTS AND DISCUSSION

The methodology carried out for the analysis of this meteorite consisted on the following strategy. First, the elemental characterization was performed by means of the acquisition of μ-EDXRF maps on both surfaces. Thanks to the μ-EDXRF maps, it was possible to establish coexistence of elements and detect hot spots of interest for the subsequent molecular characterization by means of point-by-point Raman analyses. Finally, when a trend was detected and/or if the mineral distribution was significantly interesting, Raman images were performed.

In this way, the elemental characterization was carried out in both sides of the meteorite and no elemental difference between them was observed. Figure 1 shows the 12 elements that were detected in the sample. Elements with a relative abundance higher than 10% wt. were considered as major elements, namely Fe, Si, and Mg. Ca and Al were found as minor elements with a relative abundance between 1 and 10% wt. Finally, trace elements (<1% wt.) were Mn, Cr, Ti, S, P, V, and Ni.

3.1 | Main mineral phases: Olivine, pyroxene, and plagioclase

In Figure 1, it is observed that iron and magnesium coexist in several areas, forming phenocrysts. Therefore, in order to find out what minerals were involved in those grains, Raman analyses were performed. The spectra obtained are composed by the Raman bands (Figure 2A) that appear at 140 (very weak, vw), 225 (weak, w), 304 (w), 400 (w), 436 (w), 584 (w), 625 (medium, m), 820 (very strong, vs), 849 (vs), 917 (vw), and 959 (vw) cm^{-1},[13] which correspond to the bands of olivine [$(Mg, Fe)_2SiO_4$].[13] The literature[15] confirms that the band position of the doublet (800–880 cm^{-1}) changes as a function of the Mg/(Mg + Fe) content. Thus, this fact can be used to estimate the forsterite (Fo, Mg_2SiO_4) and fayalite (Fa, Fe_2SiO_4) content in the olivine grains. Hence, according to the Torre-Fdez et al.[15] equations and after selecting the main band position of all olivine spectra obtained, the forsterite and fayalite range composition in the LAR 12095 is between $Fo_{55.0}Fa_{45.0}$ and $Fo_{60.4}Fa_{39.6}$, in agreement with literature.[12] Once the point-by-point analyses were done, a Raman map of the central area was acquired. In this way, the spectral range 814–823 cm^{-1} was selected to obtain the olivine distribution Raman image. As can be seen in Figure 2A (in blue), the distribution of olivine corresponds perfectly with the crystals showing the highest content of iron in the elemental distribution (Figure 1).

In addition, Figure 1 shows that silicon is the main element that composes the matrix. The groundmass was characterized by Raman spectroscopy and the spectrum pattern of pyroxene [$R_2(Si,Al)_2O_6$] (R: Mg, Fe, Ca, Al, Ti, Mn, Na, K, or Li)[16] (Figure 2B) was found, being present both high Ca- and low Ca-pyroxenes. Low Ca-pyroxenes seems to be predominant with Raman bands at 332 (m), 398 (m), 538 (w), 658 (shoulder, sh m), 672 (m), 940 (vw), and 1003 (vs) cm^{-1}. According to the work of Wang et al.,[17] this is a magnesium-rich pyroxene with a *Pbca* or $P2_{1/c}$ crystal structure. This is because the Raman spectrum has two doublets, one in the 650–700 cm^{-1} region and the other in the 300–400 cm^{-1} region. According to the work of Huang et al.,[18] this spectrum corresponds to a enstatite-ferrosilite orthopyroxene [$(Mg, Fe)SiO_3$]. Finally, on the Raman map carried out in the middle of the sample, the spectral interval of a characteristic pyroxene band (668–680 cm^{-1}) was selected to obtain the pyroxene Raman image (Figure 2B, in red). As seen, pyroxene can be considered the main mineral in the bulk of the meteorite in agreement with the initial results from the Meteoritical Bulletin.[7]

Several Al-rich spots (see Figure 1) were analyzed by micro-Raman spectroscopy and the spectra showed broad bands in 450–7000 cm^{-1} region, which correspond to some type of plagioclase [$NaAlSi_3O_8$-$CaAl_2Si_2O_8$].[14,19] Although Raman spectroscopy can identify different non-shocked plagioclases, the plagioclase found in this sample is clearly maskelynite, because no secondary bands in the 200–450 cm^{-1} region were found (Figure S1A).[19]

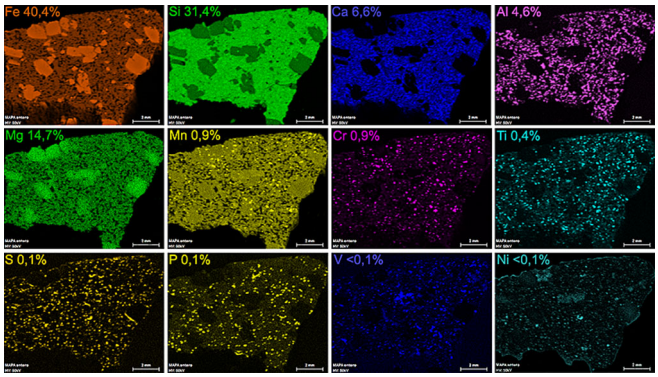

FIGURE 1 Elemental distribution of Fe, Si, Mg, Ca, Al, Mn, Cr, Ti, S, P, V, and Ni in the LAR 12095 Martian meteorite obtained by μ-EDXRF. The Fe phenocrysts are the brightest areas of the iron map, which match with those of Mg. This fact allows thinking about the presence of olivine phenocrysts.

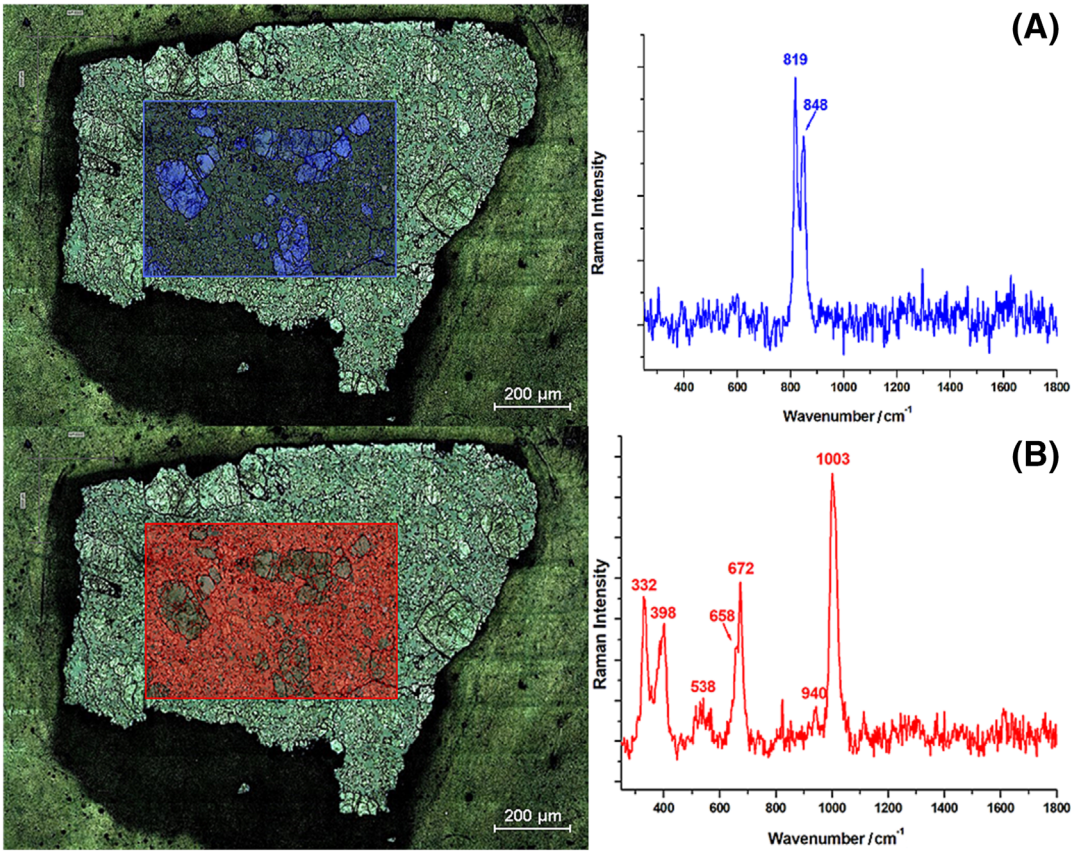

FIGURE 2 (A) Raman image of olivine and its Raman spectrum. The image was obtained using the interval 814–823 cm^{-1}. (B) Raman image of pyroxene and its Raman spectrum. The image was obtained using the interval 668–680 cm^{-1}. Both spectra were acquired with the following conditions: 532 nm laser, 1800 L/mm grating, 3 s of exposure time, 2 accumulations, 10% of laser power, 5× objective.

3.2 | Oxides: Hematite, anatase, ilmenite, and chromite

By means of both modes, single point analysis and Raman mappings, the oxides hematite [Fe_2O_3],[20] anatase [TiO_2],[21] ilmenite [$FeTiO_3$],[22] and chromite [$FeCr_2O_4$][22] were also detected.

The Raman bands position of hematite appear at 223 (w), 292 (m), 403 (m), 605 (w), and 1303 (broad and weak, bw) cm^{-1} (Figure 3D).[20] This iron oxide was unequivocally identified on Mars, for the first time, in 1996 by the Thermal Emission Spectrometer (TES) on board the Mars Global Surveyor spacecraft.[23] In fact, fine-grained hematite gives Mars its characteristic red color, the reason why this planet is called the "Red Planet." Several studies have confirmed that the presence of hematite on Mars is due to a weathering process.[23,24] That is, on Mars there are many iron-rich minerals, so that through chemical reactions, these compounds are weathered, in part, to hematite.[23,24] Thus, hematite is considered a secondary mineral from Mars.

The titanium oxide anatase[21] is a metastable mineral phase (the low temperature polymorph) of titanium dioxide, which is very well characterized and distinctive from other polymorphs by Raman spectroscopy because its peaks appear at 142 (vs), 194 (w), 396 (w), 517 (w), and 639 (m) cm^{-1} (Figure S1B).[21] It is well known that anatase is usually a secondary mineral derived from other titanium-bearing minerals. In addition, it can be derived from the weathering of rocks by hydrothermal processes or from crystal fractionation of igneous samples.[25]

In addition to hematite and anatase, other oxides were identified. The Fe-Ti-Cr-oxides have similar Raman spectra patterns, which include a main band in the 600–800 cm^{-1} range, and few minor peaks at lower wavenumbers.[22] Knowing all major and minor Raman peaks, it would be possible to distinguish between the different Fe-Ti-Cr-oxides, but when the S/N signal is low, it is quite difficult to do so. In this sample, many spectra with a strong band in the range of the Fe-Ti-Cr oxides were found and the secondary Raman bands appeared in different positions allowing us to distinguish among

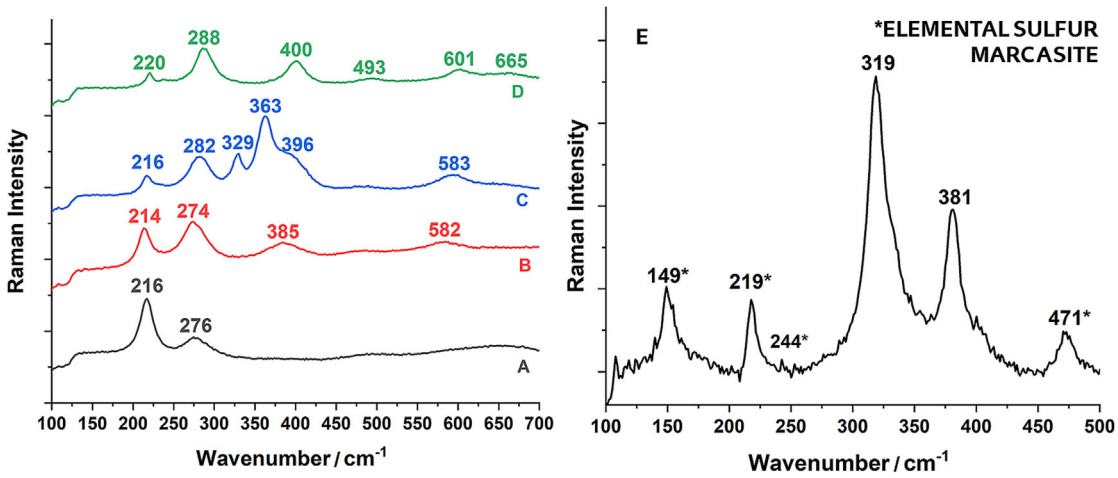

FIGURE 3 Raman spectra of (A) oxidized mackinawite, (B) oxidized mackinawite and broad iron oxide bands, (C) oxidized mackinawite, pyrrhotite, and broad iron oxide bands, (D) hematite and (E) elemental sulfur and marcasite. Measurement conditions: 532 nm excitation laser, 1800 L/mm grating, 10 s of exposure time, 10 accumulations, 10% of laser power, 50× objective.

different Fe-Ti-Cr oxides. In this sense, the first Fe-Ti-Cr oxide found features the most intense band at 686 cm^{-1}, whereas the secondary bands appear at 228 (m), 335 (m), and 376 (w) cm^{-1}, which correspond to the characteristic spectrum of ilmenite (Figure 1SC).[22] The measurement conditions: laser 532 nm, 6 s of exposure time, 20 accumulations, 5% of laser power, and objective ×5. The rover Spirit of the Mars Exploration Rover Mission detected ilmenite in the Gusev Crater of Mars by the alpha particle-X-ray spectrometer and the Mössbauer spectrometer.[26] In fact, ilmenite was detected in the same rock as pyroxene, olivine, hematite, nanophases of iron oxides, and magnetite.[26] This fact proves that ilmenite is a primary mineral from Mars.

The other Fe-Ti-Cr oxide found has a broad Raman band at 684 cm^{-1} and a secondary broad peak at 560 cm^{-1}. According to the work of Wang et al.,[22] the spectrum found matches perfectly with the chromite spectrum (Figure S1D). The Raman position of the main band reveals the molar ratio (Cr + Fe)/(Cr + Fe + Al).[22] In this case, Raman peak suggests values of 0.8–1.0. This range indicates that the chromite found may contain traces of aluminum, which is consistent because μ-EDXRF images showed that sometimes aluminum coexisted with chromium. In addition, magnesiochromite was also detected thanks to its Raman bands: 560 (m), 598 (m), 645 (s), 689 (vs), and 1363 (w, b).[13] Martian orbiters, rovers, and landers have not yet found chromite on the red planet. However, there are many Martian meteorites[22,27] with chromite present.

In addition to the major mineral phases and the oxides found, phosphates, sulfides, elemental sulfur, and sulfates were also detected as minor mineral phases.

3.3 | Phosphate

As can be seen in Figure S2A, where some elemental images were overlapping, sometimes the distribution of calcium, magnesium, and phosphorus match. In these points, the calcium phosphate merrillite [$Ca_9NaMg(PO_4)_7$][28] was detected by single Raman point mode. Its Raman spectrum is characterized by the Raman bands that appear at 354 (w), 407 (m), 958 (vs), 975 (vs), and 1111 (m) cm^{-1} (Figure S1E).[28] There is not any report about the presence of merrillite on Mars, but it is a dominant mineral in Martian meteorites. Unfortunately, the origin of its presence in meteorites is not yet fully established. Nevertheless, it is known that whitlockite (primary mineral from Mars[29]) can be transformed into merrillite by shock processes. This leads us to think that the whitlockite was transformed into merrillite in the process of meteoroid generation. Therefore, merrillite could be considered a secondary mineral from Mars.

3.4 | Sulfur-rich mineral phases

In addition to the minerals seen so far, sulfur-rich compounds were expected to be found, because the elemental images of sulfur and iron match (see Figure S2B). Almost 50 years ago, Viking missions revealed that Mars has S- and Cl-rich surface regolith, and since that time, sulfur has been confirmed by *in situ* measurements made by landers and rovers, by remote sensing observations made by orbiters, and by analyses of Martian meteorites in terrestrial laboratories.[30] It is estimated that most primary igneous sulfur is concentrated in sulfides, including

pyrrhotite, rare chalcopyrite, cubanite, troilite, pentlandite, and pyrite.[31] In addition to primary minerals, sulfur is also found in a variety of secondary mineral phases in Martian meteorites, such as secondary sulfides, sulfates, elemental sulfur, and impact glasses, among others.[31]

After understanding this, it is necessary to emphasize that the sulfur cycle dominates many geochemical processes on Mars. During the formation of Mars, sulfur was distributed in the core to form a liquid Fe-(Ni)S core. Subsequently, the transfer of S to the crust occurred through volcano degassing, magmatism, and hydrothermal processes, which resulted in a considerable amount of S at the surface. According to Huidobro et al.,[6] photochemical activity and the presence of oxidizing agents led to rapid formation of S-bearing minerals, such as sulfides. If oxidation continued on Mars without the presence of atmospheric oxygen (anaerobic conditions), the primary sulfides may have oxidized to secondary sulfides,[32] elemental sulfur, and sulfates. In contrast, if the oxidation of sulfur compounds occurs on Earth, under oxygen presence (aerobic conditions), the results is completely different, leading to the formation of iron oxides, such as hematite, goethite, lepidocrocite, among others.[32,33]

Surprisingly, both types of oxidation, aerobic and anaerobic, were observed in the LAR 12095 meteorite. First of all, mackinawite [tetragonal FeS, metastable][33] was detected and it is well known that its Raman bands appear at 208 (s), 274 (vs), and 385 (s) cm^{-1},[33] but the ones detected experimentally appear at 214 (vs), 273 (vs), and 382 (b, m) cm^{-1} (Figure 3A). Mendili et al.[32] were able to observe that mackinawite is a metastable iron sulfur and is highly susceptible to transform. In fact, it has been proven that the main mackinawite Raman bands shift toward higher wavenumbers, until the alteration causes a change in the crystal structure from tetragonal to monoclinic [pyrrhotite, FeS, stable].[32] Therefore, as the experimentally bands detected have the same structure as mackinawite but with a small displacement toward higher wavenumbers, it can be concluded that the compound found is an oxidized mackinawite (see Figure 3A).

Secondly, Figure 3B shows the oxidized mackinawite together with the 385 and 582 cm^{-1} Raman bands,[32,33] which means that the metastable iron sulfide formed in anoxic conditions on Mars has started to oxidize in the presence of oxygen, forming the appearance of the first iron oxide bands.

Thirdly, Figure 3C shows the oxidized mackinawite weathering under anaerobic conditions, where part of the mackinawite has been transformed to pyrrhotite.[32] Although the exact Raman peaks for pyrrhotite can vary as function of stoichiometry as well as with the degree of ordering, and reflect variations in the FeS bond lengths, their pattern spectrum is characterized by strong peaks close together below 400 cm^{-1}.[34] And the ones obtained in the laboratory appear at 329, 363, and 396 cm^{-1}.[35]

Finally, Figure 3D shows the hematite spectrum, which is the product of the complete alteration of iron sulfides in the presence of oxygen.

As mentioned above, anaerobic oxidation of primary sulfides with high sulfur input can produce secondary oxides or FeS_2 (pyrite or marcasite, FeS_2, stable, and metastable, respectively[6]), elemental sulfur [S_8][6] and Fe^{2+} sulfates.[36] Figure 3E shows the Raman bands of marcasite and elemental sulfur, which are 319 (vs) and 381 (s); and 149 (m), 219 (m), 244 (w), and 471 (m), respectively.[6,13]

Moreover, in this meteorite, it was observed that the oxidation in an anaerobic environment persisted. Sulfides and elemental sulfur continued to oxidize to anhydrous sulfates, which can hydrate through hydrothermal activity, leading to the formation of hydrated sulfates. In this sense, the iron sulfate jarosite [$KFe_3(SO_4)(OH)_6$][37] was detected thanks to its Raman bands that appear at 139 (m), 224 (s), 300 (m), 355 (w), 434 (vs), 454 (m), 573 (m), 625 (m), 1007 (vs), 1051 (w), 1103 (vs), and 1153 (w) cm^{-1}[38] (Figure 4). On the Earth, jarosite forms as the result of low-temperature acidic-oxidative weathering of iron-bearing minerals in water presence.[36,37] In addition,

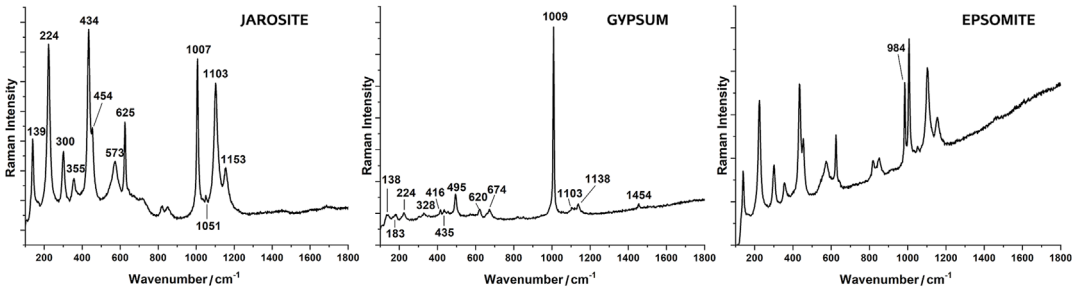

FIGURE 4 Raman spectra of jarosite, gypsum, and epsomite. Measurement conditions: 532 nm excitation laser, 1800 L/mm grating, 10 s of exposure time, 3 accumulations, 10% of laser poser, 50× objective.

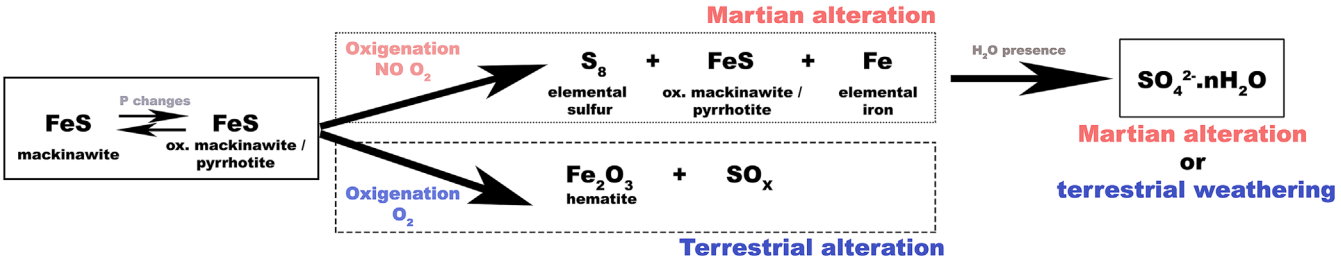

FIGURE 5 Possible alterations of primary Martian sulfides on Mars as a function of the minerals found in the LAR 12095 Martian meteorite by micro-Raman spectroscopy and micro-EDXRF.

this compound was reported in 2004 by the Opportunity rover at fine-grained sediments of Meridiani Planum.[37] Therefore, the jarosite of this meteorite can be considered as a secondary mineral as well as a weathering mineral phase.

As can be seen in Figure S2C,D, the distribution of sulfur along the meteorite also often match with the distribution of calcium and magnesium. In this way, two additional sulfates were detected by Raman spectroscopy: gypsum [$CaSO_4.2H_2O$] and epsomite [$MgSO_4.7H_2O$]. Both hydrated sulfates have been detected in Mars by the Opportunity rover, the OMEGA on the Mars Express orbiter, the Phoenix lander, the CRISM on the Mars Reconnaissance orbiter, among others.[39]

Gypsum was identified thanks to its Raman bands: 133 (w), 183 (w), 224 (w), 328 (w), 416 (w), 435 (w), 495 (m), 620 (w), 674 (w), 1009 (vs), 1103 (w), 1138 (w), and 1454 (w) cm^{-1} (Figure 4). Epsomite was detected through its main Raman band that appears at 984 (vs) cm^{-1} (Figure 4). These minerals are coming from a sulfate-alteration/evaporation process and can be formed in a wide variety of depositional environments. According to literature,[40,41] the presence of hydrated sulfates on Mars is due to sulfur-bearing water interacts with Ca/Mg-bearing minerals, leaving gypsum and epsomite as water evaporated.

Therefore, the gypsum and epsomite of this meteorite may be due to the alteration of S-bearing water and Ca-bearing minerals on Mars or on the Earth. As both mineral phases appear occasionally in some areas in the surface of the meteorite and do not have a distribution along the cracks, it seems that both sulfates are likely to have a Martian origin and that are not due to an afterwards terrestrial weathering. After ejection, both hydrated sulfates probably dehydrated, but after the meteorite landing on the Antarctica ices, both could be rehydrated again.

Thus, in the LAR 12095 Martian meteorite, it has been possible to verify once again the different stages, in which sulfur can be found from the most reduced form to the most oxidized.

All the proposed reactions can be seen shown in Figure 5. The primary Martian sulfides can follow three different pathways. The first one consist on forming secondary sulfides due to pressure changes. The second one is the anaerobic route, which occurs on Mars, due to oxidizing agents secondary sulfides, elemental sulfur and elemental iron are produced. The third possibility is that primary or secondary sulfides may be oxidized under aerobic conditions, which occurs on Earth, generating iron oxides, such as hematite, and sulfur oxides (SOx).

Finally, the elemental sulfur and the secondary sulfides can be altered until anhydrous or hydrated sulfates. This process may occur due to hydrothermal conditions on Mars or due to terrestrial weathering.

4 | CONCLUSIONS

By means of Raman experiments, performed on hotspots selected after a μ-EDXRF mapping of the surface, the LAR 12095 shergottite was geochemically characterized. It was found that the matrix of the samples was mainly composed by a groundmass of enstatite-ferrosilite orthopyroxene [$(Mg,Fe)SiO_3$] and olivine phenocrysts embedded in the matrix. Both mineral phases are classified as primary minerals. Moreover, occasionally ilmenite and iron sulfides were also found as primary mineral phases. As secondary mineral phases, maskelynite, hematite, anatase, chromite, merrillite, oxidized mackinawite, pyrrhotite, elemental sulfur, marcasite, jarosite, gypsum, and epsomite were detected.

Hematite is probably coming from the acidic-oxidative alteration of Fe-bearing mineral phases, such as iron sulfides. On the other hand, it is well known that anatase is a product of the weathering of Ti-bearing minerals under hydrothermal conditions. Even though the presence of merrillite in Martian meteorites is not yet fully proven, it is believed that merrillite comes from the alteration of whitlockite due to pressure shock during the meteorite formation.

The most novel discovery made in this meteorite was the two different paths that alterations of S-bearing minerals can take. That is, it is known that the transfer of S to the crust occurred through degassing, magmatism, and hydrothermal processes, which resulted in a considerable amount of S at the surface. Part of these gasses were oxidized under anaerobic conditions, forming the primary sulfides. At this point, the alteration of primary iron sulfides can follow two different paths, the two that have been seen in this meteorite. At this point, the alteration of primary Martian sulfides can follow two different paths, the one that occurs on Mars under anaerobic conditions and the other that occurs on Earth under aerobic conditions. According to the first path, primary sulfides transform into secondary sulfides, elemental sulfur and sulfates (under hydrothermal conditions) on Mars. Regarding the second path, primary sulfides alter into different oxides on Earth due to the oxidizing terrestrial atmosphere. The resulted mineral phases obtained in this meteorite through the first path were mackinawite, pyrrhotite, marcasite, and elemental sulfur. In contrast, iron oxides such as hematite were obtained as a result of the second alteration path.

Jarosite was reported to be on Mars by the Opportunity rover, but its presence on the red planet comes as the result of low-temperature acidic-oxidative weathering of Fe-bearing minerals in water presence. Finally, epsomite and gypsum are common sulfate-alteration/evaporation products and are formed in a wide variety of depositional environments, so they come from the interaction between S-bearing water with Ca/Mg-bearing minerals, or due to the oxidation of S-bearing primary minerals.

No minerals have been found that would certainly come from terrestrial weathering. However, the origin of chromite is not yet established, because Martian orbiters, rovers, and landers have not found chromite in Mars, and many Martian meteorites have chromite. Therefore, chromite may be a primary mineral not yet reported, a secondary mineral, or a terrestrial weathering mineral.

After this characterization, it can be said that the objectives were satisfactorily fulfilled. In addition, it has been possible to verify how micro-Raman spectroscopy (using both point-by-point and imaging modes), assisted with micro-EDXRF imaging is a fast and complete way to carry out the geochemical characterization of samples that cannot be destroyed and thus it could be used on the future characterization of Mars Returned samples from the upcoming MSR mission.

ACKNOWLEDGMENTS

All the authors are grateful to NASA for providing access to the LAR 12095 Martian meteorite sample through the loan agreement between NASA's JSC and the UPV/EHU. US Antarctic meteorite samples were collected by the Antarctic Search for Meteorites (ANSMET) program, which has been funded by National Science Foundation (NSF) and NASA, and characterized and curated by the Department of Mineral Science of the Smithsonian Institution and Astromaterials Curation Office at NASA's JSCe. Jennifer Huidobro and Iratxe Población are grateful to the Basque Government and UPV/EHU, respectively, for their pre-doctoral contracts. Julene Aramendia is grateful to the Basque Government María Zambrano contract, and Cristina García-Florentino is thankful to the UPV/EHU post-doctoral contract. This work has been supported through the Raman On Mars project: "Contribution of the Raman spectroscopy to the exploration of Mars and Martian Moons: ExoMars, Mars 2020 and MMX missions (RamOnMars)" (Grant No. PID2019-107442RB-C31), funded by the Spanish Agency for Research (through the Spanish Ministry of Science and Innovation, MICINN, and the European Regional Development Fund, FEDER), and the Strategic Project "Terrestrial and Planetary Alteration Processes" (Grant No. UPV/EHU PES18/57), funded by the UPV/EHU.

CONFLICT OF INTEREST STATEMENT

The authors declare that there is no conflict of interest that could be perceived as prejudicing the impartiality of the research reported.

ORCID

Jennifer Huidobro https://orcid.org/0000-0001-8302-8583
Cristina García-Florentino https://orcid.org/0000-0002-0329-8012
Iratxe Población https://orcid.org/0000-0002-9162-3734

REFERENCES

[1] A. Udry, G. H. Howarth, C. D. K. Herd, J. M. D. Day, T. J. Lapen, J. Filiberto, *J. Geophys. Res. Planets* **2020**, *125*, e2020JE006523.
[2] J. Huidobro, J. Aramendia, G. Arana, J. M. Madariaga, *Anal. Chim. Acta* **2022**, *1197*, 339499.
[3] A. H. Treiman, J. D. Gleason, D. D. Bogard, *Planet. Space Sci.* **2000**, *48*, 1213.
[4] K. A. Farley, K. H. Williford, K. M. Stack, R. Bhartia, A. Chen, M. de la Torre, K. Hand, Y. Goreva, C. D. K. Herd, R. Hueso, Y. Liu, J. N. Maki, G. Martinez, R. C. Moeller, A. Nelessen, C. E. Newman, D. Nunes, A. Ponce, N. Spanovich, P. A. Willis, L. W. Beegle, J. F. Bell, A. J. Brown, S.-E. Hamran, J. A. Hurowitz, S. Maurice, D. A. Paige, J. A. Rodriguez-Manfredi, M. Schulte, R. C. Wiens, *Space Sci. Rev.* **2020**, *216*, 142.
[5] C. García-Florentino, I. Torre-Fdez, P. Ruiz-Galende, J. Aramendia, K. Castro, G. Arana, M. Maguregui, S. Fdez-Ortiz de Vallejuelo, J. M. Madariaga, *Talanta* **2020**, *224*, 121863.

[6] J. Huidobro, J. Aramendia, C. García-Florentino, P. Ruiz-Galende, I. Torre-Fdez, K. Castro, G. Arana, J. M. Madariaga, *J. Raman Spectrosc.* **2022**, *53*, 450.
[7] J. Aramendia, L. Gomez-Nubla, K. Castro, S. Fdez-Ortiz de Vallejuelo, G. Arana, M. Maguregui, V. G. Baonza, J. Medina, F. Rull, J. M. Madariaga, *TrAC Trends Anal. Chem.* **2018**, *98*, 36.
[8] J. M. Madariaga, J. Aramendia, G. Arana, K. Castro, L. Gómez-Nubla, S. Fdez-Ortiz de Vallejuelo, C. Garcia-Florentino, M. Maguregui, J. A. Manrique, G. Lopez-Reyes, J. Moros, A. Cousin, S. Maurice, A. M. Ollila, R. C. Wiens, F. Rull, J. Laserna, V. Garcia-Baonza, M. B. Madsen, O. Forni, J. Lasue, S. M. Clegg, S. Robinson, P. Bernardi, A. J. Brown, P. Caïs, J. Martinez-Frias, P. Beck, S. Bernard, M. H. Bernt, O. Beyssac, E. Cloutis, C. Drouet, G. Dromart, B. Dubois, C. Fabre, O. Gasnault, I. Gontijo, J. R. Johnson, J. Medina, P.-Y. Meslin, G. Montagnac, V. Sautter, S. K. Sharma, M. Veneranda, P. A. Willis, *Anal. Chim. Acta* **2022**, *1209*, 339837.
[9] H. C. Connolly, C. Smith, G. Benedix, L. Folco, K. Righter, J. Zipfel, A. Yamaguchi, H. Chennaoui-Aoudjehane, *Meteorit. Planet. Sci.* **2007**, *42*, 1647.
[10] P. L. Clay, K. H. Joy, B. O'Driscoll, H. Busemann, L. Ruzié-Hamilton, R. Burgess, J. Fellowes, B. Joachim-Mrosko, J. Pernet-Fisher, S. Strekopytov, C. J. Ballentine, *Am. Mineral.* **2020**, *105*, 289.
[11] G. H. Howarth, Y. Liu, I. Kohl, J. F. Pernet-Fisher, C. Wetteland, Y. Chen, R. J. Bodnar, E. D. Young, L. A. Taylor, in 46th Lunar and Planetary Science Conference, **2015**, 1360.
[12] E. T. Dunham, J. B. Balta, M. Wadhwa, T. G. Sharp, H. Y. McSween, *Meteorit. Planet. Sci.* **2019**, *54*, 811.
[13] B. Lafuente, R. T. Downs, H. Yang, N. Stone, in *Highlights in mineralogical crystallography*, (Eds: T. Armsbruster, R. M. Danisi), De Gruyter, Berlin, Germany **2015**, 1.
[14] J. Fritz, V. Assis Fernandes, A. Greshake, A. Holzwarth, U. Böttger, *Meteorit. Planet. Sci.* **2019**, *54*, 1533.
[15] I. Torre-Fdez, P. Ruiz-Galende, J. Aramendia, L. Gomez-Nubla, K. Castro, G. Arana, J. M. Madariaga, in 50th Lunar and Planetary Science Conference, No. 2132, **2019**, 2486.
[16] P. M. Huang, M. K. Wang, in *Encyclopedia of soils in the environment*, 1st ed. (Ed: D. Hillel), Elsevier, Oxford, UK **2005**, 500.
[17] A. Wang, B. L. Jolliff, L. A. Haskin, K. E. Kuebler, K. M. Viskupic, *Am. Mineral.* **2001**, *86*, 790.
[18] E. Huang, C. H. Chen, T. Huang, E. H. Lin, J. Xu, *Am. Mineral.* **2000**, *85*, 473.
[19] S. Shkolyar, S. J. Jaret, B. A. Cohen, J. R. Johnson, O. Beyssac, J. M. Madariaga, R. C. Wiens, A. Ollila, S. Holm-Alwmark, Y. Liu, *Earth. Moon. Planets* **2022**, *126*, 4.
[20] A. Zoppi, C. Lofrumento, E. M. Castellucci, M. G. Migliorini, *Ann. Chim.* **2005**, *95*, 239.
[21] E. S. Araújo, J. Libardi, P. M. Faia, H. P. de Oliveira, *J. Chem.* **2015**, *2015*, 1.
[22] A. Wang, K. E. Kuebler, B. L. Jolliff, L. A. Haskin, *Am. Mineral.* **2004**, *89*, 665.
[23] P. R. Christensen, R. V. Morris, M. D. Lane, J. L. Bandfield, M. C. Malin, *J. Geophys. Res. Planets* **2001**, *106*, 23873.
[24] D. C. Catling, J. M. Moore, *Icarus* **2003**, *165*, 277.
[25] V. Muñoz-Iglesias, L. Sánchez-García, D. Carrizo, A. Molina, M. Fernández-Sampedro, O. Prieto-Ballesteros, *Sci. Rep.* **2022**, *12*, 5640.
[26] S. W. Squyres, R. E. Arvidson, J. F. Bell, J. Brückner, N. A. Cabrol, W. Calvin, M. H. Carr, P. R. Christensen, B. C. Clark, L. Crumpler, D. J. D. Marais, C. D'Uston, T. Economou, J. Farmer, W. Farrand, W. Folkner, M. Golombek, S. Gorevan, J. A. Grant, R. Greeley, J. Grotzinger, L. Haskin, K. E. Herkenhoff, S. Hviid, J. Johnson, G. Klingelhöfer, A. Knoll, G. Landis, M. Lemmon, R. Li, M. B. Madsen, M. C. Malin, S. M. McLennan, H. Y. McSween, D. W. Ming, J. Moersch, R. V. Morris, T. Parker, J. W. Rice, L. Richter, R. Rieder, M. Sims, M. Smith, P. Smith, L. A. Soderblom, R. Sullivan, H. Wänke, T. Wdowiak, M. Wolff, A. Yen, *Science (80-.)* **2004**, *305*, 794.
[27] A. Lagain, S. Bouley, B. Zanda, K. Miljković, A. Rajšić, D. Baratoux, V. Payré, L. S. Doucet, N. E. Timms, R. Hewins, G. K. Benedix, V. Malarewic, K. Servis, P. A. Bland, *Nat. Commun.* **2022**, *13*, 3782.
[28] M. Jia, K. Zhai, M. Gao, W. Wen, Y. Liu, X. Wu, S. Xhai, *Vib. Spectrosc.* **2020**, *106*, 103005.
[29] C. T. Adcock, O. Tschauner, E. M. Hausarth, A. Udry, S. N. Lou, Y. Cai, M. Ren, A. Lanzirotti, M. Newville, M. Kunz, C. Lin, *Nat. Commun.* **2017**, *8*, 14667.
[30] H. B. Franz, P. L. King, F. Gaillard, in *Volatiles in the Martian crust*, Elsevier, Amsterdam **2019**, 119.
[31] P. L. King, S. M. McLennan, *Elements* **2010**, *6*, 107.
[32] Y. El Mendili, A. Abdelouas, J.-F. Bardeau, *Phys. Chem. Chem. Phys.* **2013**, *15*, 9197.
[33] G. Genchev, A. Erbe, *J. Electrochem. Soc.* **2016**, *163*, C333.
[34] B. Wopenka, *Meteorit. Planet. Sci.* **2012**, *47*, 565.
[35] R. H. Lara, M. G. Monroy, M. Mallet, M. Dossot, M. A. González, R. Cruz, *Environ. Earth Sci.* **1849**, *2015*, 73.
[36] P. L. King, H. Y. McSween, *J. Geophys. Res.* **2005**, *110*, E12S10.
[37] G. Baccolo, B. Delmonte, P. B. Niles, G. Cibin, E. Di Stefano, D. Hampai, L. Keller, V. Maggi, A. Marcelli, J. Michalski, C. Snead, M. Frezzotti, *Nat. Commun.* **2021**, *12*, 436.
[38] A. V. Sergeeva, *J. Appl. Spectrosc.* **2019**, *86*, 371.
[39] A. Wang, W. C. Feldman, M. T. Mellon, M. Zheng, *Icarus* **2013**, *226*, 980.
[40] K. E. Fishbaugh, F. Poulet, V. Chevrier, Y. Langevin, J.-P. Bibring, *J. Geophys. Res.* **2007**, *112*, E07002.
[41] J. S. Marion, G. M. Kargel, in Lunar and Planetary Science 2005, **2005**, 2290.

SUPPORTING INFORMATION

Additional supporting information can be found online in the Supporting Information section at the end of this article.

How to cite this article: J. Huidobro, J. Aramendia, C. García-Florentino, I. Población, K. Castro, G. Arana, J. M. Madariaga, *J Raman Spectrosc* **2023**, *54*(11), 1248. https://doi.org/10.1002/jrs.6558